IOP Publishing Journal of Physics: Condensed Matter
J. Phys.: Condens. Matter **27** (2015) 354103 (13pp) doi:10.1088/0953-8984/27/35/354103

Consistent rationalization of type-2 topoisomerases' unknotting, decatenating, supercoil-relaxing actions and their scaling relation

Zhirong Liu[1] **and Hue Sun Chan**[2]

[1] College of Chemistry and Molecular Engineering, Center for Quantitative Biology and Beijing National Laboratory for Molecular Sciences, Peking University, Beijing 100871, People's Republic of China
[2] Departments of Biochemistry, Molecular Genetics and Physics, University of Toronto, Toronto, Ontario M5S 1A8, Canada

E-mail: LiuZhiRong@pku.edu.cn and chan@arrhenius.med.toronto.edu

Received 13 December 2014, revised 15 February 2015
Accepted for publication 23 February 2015
Published 20 August 2015

Abstract

How type-2 topoisomerases discern global topology from local properties of DNA is not known precisely but the hypothesis that the enzymes selectively pass double-helix strands at hook-like juxtapositions is promising. Building upon an investigation of unknotting and decatenating using an improved wormlike DNA model, here we focus primarily on the enzymes' action in narrowing the distribution of linking number (Lk) in supercoiled DNA. Consistent with experiments, with selective passage at a hooked juxtaposition, the simulated narrowing factor R_{Lk} diminishes with decreasing DNA circle size but approaches an asymptotic $R_{Lk} \approx 1.7$–1.8 for circle size $\gtrsim$3.5 kb. For the larger DNA circles, we found that $(R_{Lk} - 1) \approx 0.42 \log_{10} R_{\rm K} \approx 0.68 \log_{10} R_{\rm L}$ and thus $R_{\rm K} \approx (R_{\rm L})^{1.6}$ holds for the computed R_{Lk} and knot and catenane reduction factors $R_{\rm K}$ and $R_{\rm L}$ attained by selective passage at different juxtaposition geometries. Remarkably, this general scaling relation is essentially identical to that observed experimentally for several type-2 topoisomerases from a variety of organisms, indicating that the different disentangling powers of the topoisomerases likely arise from variations in the hooked geometries they select. Taken together, our results suggest strongly that type-2 topoisomerases recognize not only the curvature of the G-segment but also that of the T-segment.

Keywords: wormlike DNA model, writhe, hooked-juxtaposition hypothesis, the bend-angle model

(Some figures may appear in colour only in the online journal)

1. Introduction

DNA can form knots, links, and supercoils *in vivo*. Proper cellular function requires DNA topology to be regulated [1–6] by enzymes known as topoisomerases [7]. Type-2 topoisomerases (abbreviated as topoIIs below) are a class of such enzymes that bind a double-stranded DNA (the G-segment) and pass another double-stranded DNA (the T-segment) through a G-segment break that the enzyme intially creates and subsequently religates after passage of the T-segment [8, 9]. Experiments show that topoIIs can achieve very significant topological simplification. For instance, seminal studies by Rybenkov *et al* demonstrate that some topoIIs reduce knots among DNA circles by as much as 90 times relative to topological equilibrium, where the latter baseline situation is defined by a conformational ensemble in

which double-stranded DNA segments can freely pass each other [10]. This observation implies that the strand passages effectuated by topoIIs are selective. In view of the small size of a topoII relative to the much larger DNA that the enzyme acts upon, a long-standing puzzle is whether a single topoII action involves multiple interactions with the DNA in order to ascertain global topological information of the DNA or the topoII has the ability to glean this information from local conformational features of the DNA. Mathematics and physical theory are fundamental to a solution to this puzzle. Experiments are clearly essential; but they are not sufficient by themselves. Even as we look forward to the day when the molecular structures and dynamic actions of topoIIs are fully delineated, why such actions should result in significant topological simplification still would not be obvious in the absence of theory.

The full picture of topoII action still eludes us but the gaps in our knowledge are being closed by significant recent experimental progress on topoII structure [11–17] and function [13, 14, 17–25]. On the theory side, since the original observation by Rybenkov *et al*, several competing hypothetical topoII mechanisms have been proposed [10, 26–38]; but now the theoretical possibilities have been narrowed down by recent experimental advances [19, 20, 22, 24, 25]. Specifically, the tracking model [10] was disproved [19]. The three-segment interaction model [32] was refuted by experiment [19]; the non-viability of this model has since been confirmed by the model's original proponents [24]. The kinetic proofreading model [27, 29] has been ruled out recently as well [22]. These developments leave the bend-angle [26, 28, 30, 36] and hooked-juxtaposition [31, 33–35, 37, 38] models as the only remaining viable candidates among the hypothesized topoII mechanisms. Both of these hypotheses postulate that local DNA conformational properties are sufficient for inferring global DNA topology. Both posit that curvature of the G-segment is important for topoII action, which is consistent with recent structural and functional studies by mutational experiments [13, 17] indicating that 'stabilization of a highly curved DNA geometry is critical to the type IIA topoisomerase catalytic cycle' [17]. The most important difference between the two hypotheses is that the hooked-juxtaposition hypothesis envisions topoII actions depending also on the curvature of the T-segment (topoIIs only act on G- and T-segments that curve toward each other [31]) whereas the bend-angle hypothesis does not. It appears from recent experiments that the hooked-juxtaposition hypothesis holds more promise because G-segment bending is insufficient by itself to account for the divergence in disentangling activities among different topoIIs [20, 25]. Several experiment show further that topoII action involves T-segment selection [11, 12, 24]. Although it is not yet clear what properties of the T-segment is being selected, the existence of such a selection adds tentative support for the hooked-juxtaposition hypothesis.

The ability of the hooked-juxtaposition mechanism [31] to produce significant unknotting and decatenating effects that are consistent with a broad range experiments was first verified by studies of DNA chains configured on simple cubic lattices [33, 34]. Lattice and other simplified chain representations [39] have proven useful in the study of knot theory [40–45] and DNA topology [46–48] as well as in simplified modeling of protein folding [49, 50] and evolution [51]. As noted by us [33, 34] and others [36], many structural and energetic details of DNA are neglected in the highly coarse-grained lattice models. Nonetheless, a subsequent assessment of the hooked-juxtaposition hypothesis [37] using an improved wormlike chain model for DNA [52, 53] leads to very similar results [33, 34]. The same wormlike DNA simulation also indicates that the bend-angle model [28, 30, 36] cannot provide sufficently high unknotting power [37] commensurate with that observed experimentally [10]. In this context, two particularly intriguing insights [54–56] are that the robust discriminating power of a hook-like juxtaposition for unknotting is likely associated with their position in ideal knots [54, 57], and that tightening of catenanes and knots by supercoiling can significantly facilitate decatenating and unknotting by topoIIs via a hooked-juxtaposition mechanism [55, 56, 58].

The supercoil relaxing action of topoIIs has also been studied using lattice models [38]. TopoIIs narrow the distribution of linking number Lk of DNA circles [10, 19, 32] but the effect seems to diminish with decreasing DNA circle size [19, 32]. The supercoil-relaxing power of a topoII is known to correlate with its unknotting and decatenating power [10], so much so that it is common to characterize the disentangling power of a topoII by measuring only its supercoil-relaxing activity [19, 20, 24, 32]. Lattice model simulations demonstrate that selective strand passage at hooked or twisted-hooked juxtapositions can rationalize these experimental observations [38]. In contrast to a prior suggestion that a diminishing supercoil-relaxing activity with DNA circle size is inconsistent with the hooked juxtaposition hypothesis [19], a lattice analyses clarifies that such a phenomenon is a logical consequence of a hooked-juxtaposition mechanism because of writhe cancellation in small DNA circles with a hooked juxtaposition [38]. This qualitative and semi-quantitative success of the lattice model in accounting for topoII supercoil-relaxing actions provides strong support for the hooked-juxtaposition hypothesis. However, the supercoil-relaxing power R_{Lk} predicted by the lattice model is appreciably less than that observed experimentally. Moreover, although a good correlation is observed between model supercoil-relaxing activity and the unknotting and decatenating activities, the dependence of supercoil-relaxing activity on the corresponding unknotting or decatenating acitivity in the lattice model is weaker than that seen in experiments [38]. Recognizing that these shortcomings may likely be artefacts of the extremely coarse-grained lattice approach, here we apply our wormlike DNA model [52] to study the quantitative effects of strand passages on Lk distribution and to re-examine the relationship between supercoil-relaxing and unknotting and decatenating actions in the same wormlike model [37]. As shown below, the hooked-juxtaposition hypothesis is able to provide a consistent rationalization for a broad range of experimental data on topoII function with quantitative accuracy.

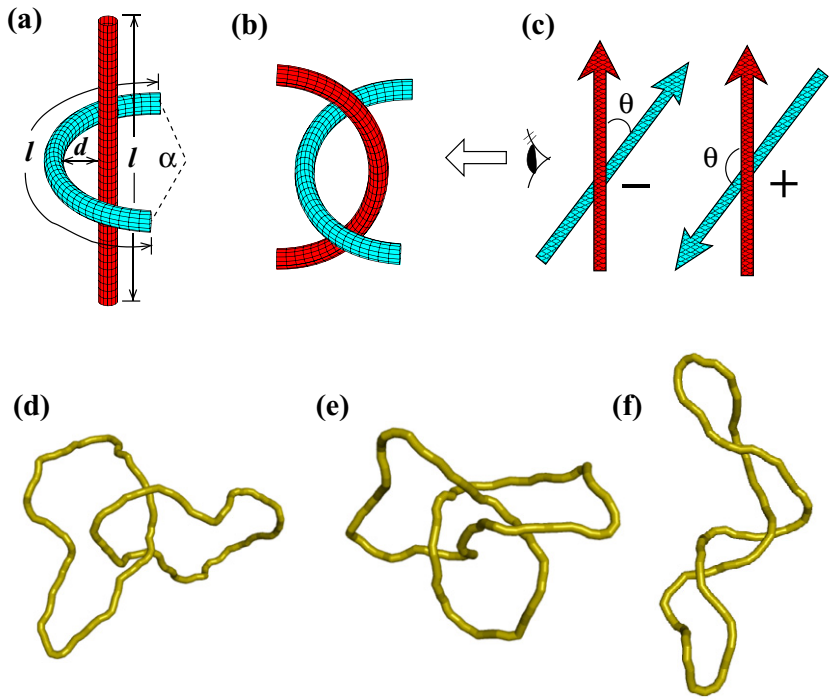

Figure 1. Model DNA juxtapositions. Topological effects of selective strand (segment) passage at various juxtaposition geometries are investigated in the present study as models for topoII actions. (*a*) A half-hooked juxtaposition. The two segments of a juxtaposition are drawn in different colors for clarity. The measure d is the midpoint separation between two segments of the juxtaposition with equal length l, and α is the arc angle subtended by the circular segment. (*b*) A hooked juxtaposition. (*c*) Sideviews of the juxtapositions in (*a*) and (*b*) showing the crossing angle θ for a negative (−) and a positive (+) crossing. The present model assumes that the pair of juxtapositions with a given geometry but of opposite signs (as shown here) are both selected with nonzero probabilities for strand passage, but the two juxtapositions in a pair need not be selected with the same favorability. The specific half-hooked and hooked juxtapositions considered in figures 2–4 correspond to the case with $d = 5$ nm, $l = 10$ nm, $\alpha = 150^\circ$ for the curved segment(s), and $\theta = 90^\circ$. (*d*)–(*f*) Example of DNA circles in our wormlike chain model. (*d*) A catenane. (*e*) A trefoil knot. (*f*) A supercoil with significant writhe. The DNA circle sizes in (*d*)–(*f*) are 1.5, 2.25, and 1.5 kb respectively. A low ionic strength equivalent to [NaCl] = 0.01 M is used to simulate these conformations so that their topological features are more apparent.

2. Model and method

2.1. The juxtaposition-centric approach in a wormlike DNA model

We apply the general approach detailed in [37, 38, 52] to the present study. In particular, DNA circles are modeled by the wormlike chain model described previously [37, 52]. This modeling setup contains an improved excluded volume term as well as a special-purpose Monte Carlo algorithm that include generalized Madras–Orlitsky–Shepp moves and length-changing moves to facilitate conformational sampling across different DNA topologies under the constraint of a preformed juxtaposition. Constrained sampling is a key feature of our juxtaposition-centric approach that allows for efficient determination of topological effects of segment passages at any given juxtaposition geometry [33, 34, 52]. The ionic strength of the solvent is modeled by varying electrostatic screening [52]. We consider both low and high ionic strengths corresponding, respectively, to [NaCl] = 0.01 M and 0.154 M [37].

Our variable juxtaposition geometries for selective strand passage follow that in [37] (figure 1). The design of these juxtapositions was motivated partly by the structure of a topoII-DNA complex reported in [13] showing that the DNA segment interacting with the topoII enzyme has length $l \approx 10$ nm and is bent into an arc subtending an angle of $\alpha \approx 150^\circ$. This approximate degree of curvature of the bound DNA G-segment is in line with more recent experimental findings [17, 20, 25]. Excluded volume and electrostatic interactions of the wormlike DNA model itself are also operative in both segments of a preformed juxtaposition. The elastic bond angle potential E_b applies as well across the connection between the preformed juxtaposition and the rest of the DNA.

The present work pays special attention to the hooked and half-hooked juxtapositions as representative geometries. As in [37], these juxtapositions are defined by $d = 5$ nm, $l = 10$ nm, and crossing angle $\theta = 90^\circ$. The arc angle $\alpha = 150^\circ$ for both segments in the hooked juxtaposition and the curved segment of the half-hooked juxtaposition, whereas $\alpha = 0^\circ$ for the straight segment of the half-hooked juxtaposition. Beside these two juxtapositions, segment passages at many other juxtaposition geometries are explored by varying d, l, θ, and α.

2.2. Effect of strand passage on the width of Lk distribution

The main task at hand is to determine the supercoil distribution narrowing factor

$$R_{Lk} = \frac{(\sigma_{Lk})^2}{[(\sigma_{Lk})_{\rm st}]^2} \qquad (1)$$

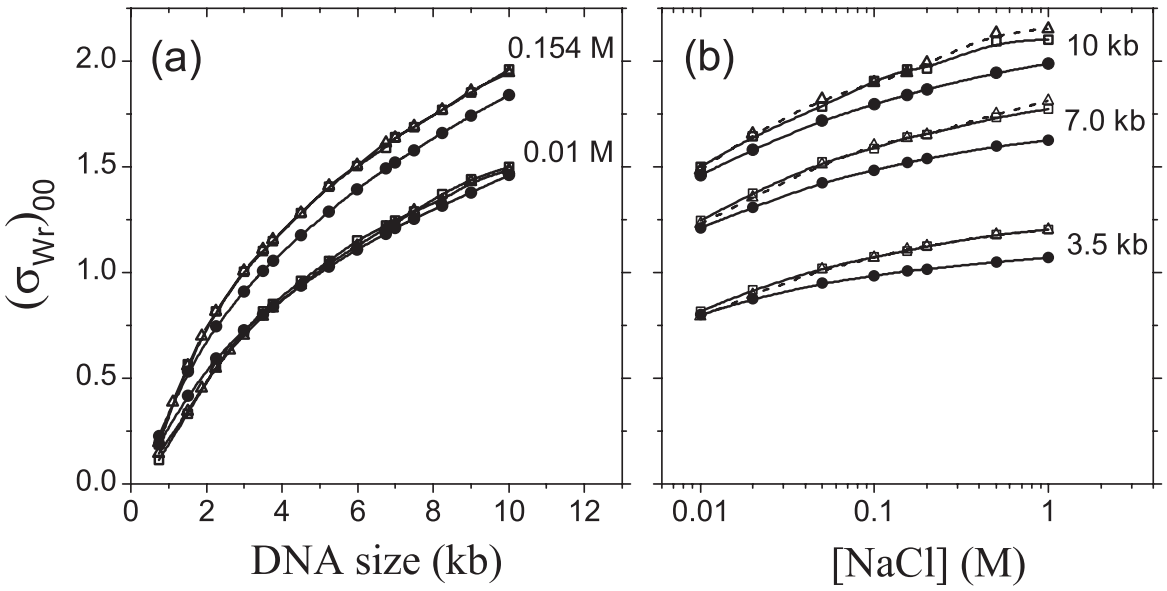

Figure 2. Standard deviation $(\sigma_{Wr})_{00}$ of writhe Wr among wormlike DNA circles with zero torsional energy ($C = 0$). Data points are shown for DNA circles with no constraint (circles), a hooked juxtaposition (squares), and a half-hooked juxtaposition (triangles). Data points are connected by solid (circles and squares) and dashed (triangles) lines as guides for the eye. (*a*) $(\sigma_{Wr})_{00}$ as a function of DNA circles sizes for ionic strengths equivalent to [NaCl] = 0.154 M (top curves) and 0.01 M (bottom curves). (*b*) $(\sigma_{Wr})_{00}$ as a function of ionic strength for DNA circle sizes of 10, 7.0, and 3.5 kb.

effectuated by selective strand passages at various juxtaposition geometries, where $(\sigma_{Lk})^2$ is the variance of the distribution $P_{\rm eq}(Lk)$ of Lk under topological equilibrium and $[(\sigma_{Lk})_{\rm st}]^2$ is the variance of the steady-state distribution $P_{\rm st}(Lk)$ maintained by selective strand passage [38]. This definition of R_{Lk} is identical to that in Rybenkov *et al* [10], Martínez-García *et al* [24], and the R parameter in Stuchinskaya *et al* [19], whereas it is the reciprocal of the $\langle\Delta Lk^2\rangle^{\rm S}/\langle\Delta Lk^2\rangle^0$ expression in Trigueros *et al* [32].

We follow the formulation in [38] and begin by simulating the distribution $P_{00}(Wr)$ of writhe Wr for wormlike DNA circles with no torsional energy for both unconstrained circles and circles constrained by a preformed juxtaposition. The computation is carried out for various juxtaposition geometries, circle sizes, and solvent conditions to determined the corresponding standard deviation $(\sigma_{Wr})_{00}$ of the zero-torsional-energy Wr distribution under those conditions. Examples of $(\sigma_{Wr})_{00}$ are given in figure 2. This quantity is of central importance in our analysis because the standard deviation σ_{Lk} of the linking number Lk under topological equilibrium is a function only of $(\sigma_{Wr})_{00}$ and the torsional energy of the DNA model [38, 52]. Once $(\sigma_{Wr})_{00}$ is known and the torsional energy C is given, σ_{Lk} is determined by the relation

$$\sigma_{Lk} = \left(1 + \frac{nl_0k_{\rm B}T}{4C\pi^2[(\sigma_{Wr})_{00}]^2}\right)^{1/2} (\sigma_{Wr})_{00} \,, \qquad (2)$$

where n is the number of segments with length $l_0 = 5$ nm in the wormlike model (see equation (17) of [38] and equation (8) of [52]). Following [37, 52], we adopt $C = 48.0k_{\rm B}T_0$ nm where $k_{\rm B}$ is Boltzmann constant and the absolute temperature $T_0 = 298$ K is used in the present study. Under these conditions, $nl_0k_{\rm B}T/4C\pi^2 = 0.615$ and 1.760, respectively, for 3.5 kb ($n = 233$) and 10 kb ($n = 667$) DNA circles.

The linking number Lk is necessarily an integer. As derived in [38], the ratio

$$S(Lk) \equiv \frac{P_{\rm st}(Lk)}{P_{\rm eq}(Lk)} \,, \qquad (3)$$

is given by

$$S(Lk) = \frac{P_{j(\mp)}(Lk \mp 2)}{P_{j(\pm)}(Lk)} \frac{P_{j(\mp)}(Lk \mp 4)}{P_{j(\pm)}(Lk \mp 2)} \cdots \frac{P_{j(\mp)}(0)}{P_{j(\pm)}(\pm 2)} \left(\frac{b_{j(-)}\rho_{j(-)}}{b_{j(+)}\rho_{j(+)}}\right)^{Lk/2} S(0) \,, \qquad (4)$$

for even $Lk \neq 0$, where $j(+)$ and $j(-)$ are the juxtapositions with positive and negative crossing selected for strand passage to maintain $P_{\rm st}(Lk)$ in the steady state. $P_{j(+)}(Lk)$ and $P_{j(-)}(Lk)$ are normalized distributions, respectively, of the number of $j(+)$ and $j(-)$ as a function of Lk. These quantities are determined by conformational sampling with a preformed juxtaposition. The factors $b_{j(+)}$, $b_{j(-)}$ are the rates of strand passage, and $\rho_{j(+)}$, $\rho_{j(-)}$ are the densities, respectively, of $j(+)$ and $j(-)$. The ρ factors account for the total number of $j(+)$ or $j(-)$ in the entire conformational ensemble, including in their counts the possible multiple appearances of a given juxtaposition geometry in one conformation. By definition [38], $\rho_{j(+)}$ and $\rho_{j(-)}$ are the average number of the given juxtaposition per equilibrium conformation and thus are independent of Lk. We find it physically reasonable to assume, as a first approximation [38], that $b_{j(+)}$ and $b_{j(-)}$ are also independent of Lk.

In equation (4), the top and bottom signs in $\mp$ and $\pm$ apply,[3] respectively, for $Lk > 0$ and $Lk < 0$. Similarly, for

odd $Lk \neq \pm 1$,

$$S(Lk) = \frac{P_{j(\mp)}(Lk \mp 2)}{P_{j(\pm)}(Lk)} \frac{P_{j(\mp)}(Lk \mp 4)}{P_{j(\pm)}(Lk \mp 2)} \cdots \frac{P_{j(\mp)}(\pm 1)}{P_{j(\pm)}(\pm 3)} \left(\frac{b_{j(-)}\rho_{j(-)}}{b_{j(+)}\rho_{j(+)}} \right)^{(Lk \mp 1)/2} S(\pm 1) \,, \tag{5}$$

where the top and bottom signs in $\mp$ and $\pm$ apply, respectively, to $Lk > 1$ and $Lk < -1$.

A simplification of the expression in equation (4) is made possible in [38] by observing that $(\sigma_{Wr})_{00}$ and therefore σ_{Lk} is approximately constant irrespective of whether the DNA circles are unconstrained or contain a preformed juxtaposition ($\sigma_{Lk} \approx \sigma_{Lk}^{(j)}$). This approximation holds for the lattice conformations in [38] and also for the present wormlike circles at high ionic strengths (figure 2). Some deviations between unconstrained and constrained $(\sigma_{Wr})_{00}$ values are seen at low ionic strengths and larger circle sizes (figure 2), but the deviations are small relative to the $(\sigma_{Wr})_{00}$ values themselves. Thus, for simplicity, we apply the same approximation uniformly here to arrive at the simplification

$$S(Lk) = \exp\left[-\frac{1}{2(\sigma_{Lk})^2} \left\{ \left[\frac{\langle Lk \rangle_{j(+)} - \langle Lk \rangle_{j(-)}}{2} - 1 \right] \times \left(Lk \mp 1 \right) \left[Lk \pm 1 - \left(\langle Lk \rangle_{j(+)} + \langle Lk \rangle_{j(-)} \right) \right] \right\} \right] \times \left(\frac{b_{j(-)}\rho_{j(-)}}{b_{j(+)}\rho_{j(+)}} \right)^{(Lk \mp 1)/2} S(\pm 1) \tag{6}$$

of equation (5) that is applicable to all odd Lk (top sign for $Lk \geqslant 1$ and bottom sign for $Lk \leqslant 1$), where $\langle Lk \rangle_{j(+)}$ is the average linking number among DNA circles containing the preformed juxtaposition $j(+)$ and $\langle Lk \rangle_{j(-)}$ is the corresponding average for the preformed juxtaposition $j(-)$. This expression and the corresponding expression for even Lk in equation (20) of [38] (which applies to all even values of Lk including $Lk = 0$) lead to the same general proportionality relation

$$P_{\rm st}(Lk) = S(Lk) P_{\rm eq}(Lk) \propto \exp\left[-\frac{\langle Lk \rangle_{j(+)} - \langle Lk \rangle_{j(-)}}{4(\sigma_{Lk})^2} \times \left\{ (Lk)^2 - 2(Lk) \left(\frac{\langle Lk \rangle_{j(+)} + \langle Lk \rangle_{j(-)}}{2} - \frac{\langle Lk \rangle_{j(+)} + \langle Lk \rangle_{j(-)}}{\langle Lk \rangle_{j(+)} - \langle Lk \rangle_{j(-)}} + \frac{(\sigma_{Lk})^2 \ln(b_{j(-)}\rho_{j(-)}/b_{j(+)}\rho_{j(+)})}{\langle Lk \rangle_{j(+)} - \langle Lk \rangle_{j(-)}} \right) \right\} \right] \tag{7}$$

given by equation (21) in [38]. The exponential term quadratic in Lk in this Gaussian distribution implies that

$$[(\sigma_{Lk})_{\rm st}]^2 = \frac{2(\sigma_{Lk})^2}{\langle Lk \rangle_{j(+)} - \langle Lk \rangle_{j(-)}} \,. \tag{8}$$

[3] This relation is equivalent to equation (6) in [38]. We note that the $P_{j(\pm)}(\mp 2)$ term in that original equation should be $P_{j(\pm)}(\pm 2)$ as in equation (4) here. This typographical error has no bearing on the other results in [38].

Hence, by the definition in equation (1),

$$R_{Lk} = \frac{\langle Lk \rangle_{j(+)} - \langle Lk \rangle_{j(-)}}{2} \,. \tag{9}$$

We use equation (9) to compute the supercoil narrowing factor.[4] Because $\langle Lk \rangle_j = \langle Wr \rangle_{00,j}$ where $\langle Wr \rangle_{00,j}$ is the average writhe among zero-torsional-energy DNA circles with preformed juxtaposition j [38], $R_{Lk} = (\langle Wr \rangle_{00,j(+)} - \langle Wr \rangle_{00,j(-)})/2$ is readily computed by juxtaposition-centric simulations of relaxed DNA circles. It follows also that the R_{Lk} predicted in the present formulation is independent of the torsional energy used in the wormlike DNA model. We adopt a working assumption that a topoII recognizes an overall juxtaposition shape and acts on both chiralities of a selected juxtaposition, although it is possible that strand passage can proceed at different rates for the two crossings with opposite signs [23, 59] (i.e. $b_{j(+)} \neq b_{j(-)}$). Accordingly, unless specified otherwise, for each selected juxtaposition in our simulation that has a positive crossing with angle θ, the negative crossing with the same d, l, and α but with crossing angle $180^\circ - \theta$ is also selected. Thus, for the example in figure 1(*c*), both juxtapositions with opposite signs are selected. Because $b_{j(+)}$, $\rho_{j(+)}$, $b_{j(-)}$, and $\rho_{j(-)}$ do not enter into the expression for $(\sigma_{Lk})_{\rm st}$, the $b_{j(-)}\rho_{j(-)}/b_{j(+)}\rho_{j(+)}$ ratio does not affect R_{Lk} as long as both $j(+)$ and $j(-)$ are selected for strand passage (i.e. $b_{j(+)}, b_{j(-)} \neq 0$). However, the $b_{j(-)}\rho_{j(-)}/b_{j(+)}\rho_{j(+)}$ ratio does affect the average steady-state linking number $\langle Lk \rangle_{\rm st}$ [38] because $b_{j(-)}\rho_{j(-)}/b_{j(+)}\rho_{j(+)}$ is part of the exponential term in equation (7) that is linear in Lk (see equation (22) of [38]).

2.3. Juxtaposition density, strand-passage rate and chiral sensing

An intuitive consideration of chain connectivity and conformational entropy suggests that in figure 1(*c*), the positive crossing (right) should be more populated than the negative crossing (left) among relaxed DNA circles because there is more conformational freedom to join the head of an arrow to the tail end of the other arrow in a positive crossing with $\theta > 90^\circ$ than a negative crossing with $\theta < 90^\circ$. In other words, in the notation of figure 1, one expects the relation $\rho_{j(+)}(\theta > 90^\circ) > \rho_{j(-)}(180^\circ - \theta)$ or equivalently $\rho_{j(-)}(\theta < 90^\circ) < \rho_{j(+)}(180^\circ - \theta)$ among juxtaposition densities. Likewise, one expects $\rho_{j(+)}(\theta < 90^\circ) < \rho_{j(-)}(180^\circ - \theta)$ or equivalently $\rho_{j(-)}(\theta > 90^\circ) > \rho_{j(+)}(180^\circ - \theta)$. If one assumes $b_{j(+)} = b_{j(-)}$, then $\langle Lk \rangle_{\rm st}$ increases with increasing $\ln(\rho_{j(-)}/\rho_{j(+)})$ [38]. Under this assumption and the above working assumption that topoIIs recognize both crossings of the same overall shape, if $\theta < 90^\circ$

[4] If the small difference between σ_{Lk} and $\sigma_{Lk}^{(j)}$ noted above is taken into account, the supercoil distribution narrowing factor may be given more accurately by $R_{Lk} + \gamma(R_{Lk} - 1)$ where R_{Lk} is given by equation (9) and $\gamma \equiv (\sigma_{Lk})^2/(\sigma_{Lk}^{(j)})^2 - 1$. For instance, using equation (2) and the data in figure 2, the computed supercoil narrowing factor of 10 kb circles in [NaCl] = 0.154 M would be increased accordingly by approximately 0.06 and 0.04, respectively, for the hooked and half-hooked juxtapositions. Detailed considerations of this and other subtle effects such as those related to the $b_{j(\pm)}$ factors—as discussed only briefly in this article—are left for future investigations.

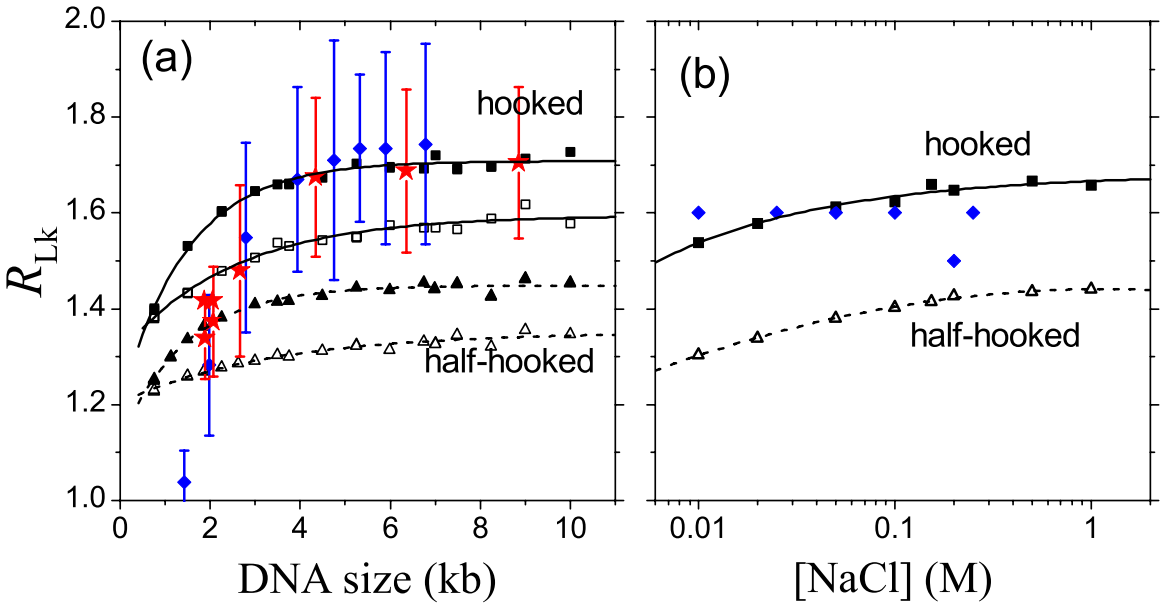

Figure 3. Narrowing of Lk distribution by selective strand passages at hooked and half-hooked juxtapositions. Solid and dashed curves are fitted through the simulated data points as guides for the eye. (a) Simulated R_{Lk} values for the hooked (black squares) and half-hooked (black triangles) juxtapositions for ionic strengths equivalent to [NaCl] = 0.154 M (filled symbols in black) and 0.01 M (open symbols) are shown as functions of DNA circle size. Included for comparison are experimental data from Trigueros *et al* (blue diamonds and associated error bars) for eukaryotic DNA topoisomerase II of *S cerevisiae* (lower panel of figure 2(D) in [32]) and from Stuchinskaya *et al* (red stars and associated error bars) for prokaryotic *E. coli* topo IV (figure 4(a) in [19]). (b) Simulated R_{Lk} values for the same juxtapositions and 3.5 kb DNA circles are shown as functions of ionic strength (black squares and triangles). Included for comparison are experimental R_{Lk} of yeast topoisomerase II as a function of [KCl] (blue diamonds) determined by Martínez-García *et al* for 7.9 kb plasmid at 37 °C (figure S1(B) of [24]).

for $j(-)$, $\rho_{j(-)}/\rho_{j(+)} < 1$, and thus positive supercoils would be preferentially removed. On the other hand, if $\theta < 90°$ for $j(+)$, $\rho_{j(-)}/\rho_{j(+)} > 1$, and thus negative supercoils would be preferentially removed.

These scenarios and broader applications of our model should be investigated in the future in view of the experimental observation that some topoIIs relax positive supercoils much faster than negative supercoils [59]. Positive and negative DNA supercoils are physically and biologically inequivalent (reviewed in [60]). The chiral sensing ability of these topoIIs is likely underpinned by the structural/energetic distinction between positive and negative DNA juxtapositions, as crossovers of opposite chiralities involve different sterics and thus have significantly different stabilities [61]. Recent experimental measurements indicate that chiral discrimination can originate from the enzymes' higher processivity [18] or higher strand-passage rate [23] for positively supercoiled DNA. In our framework, the latter behavior corresponds directly to $b_{j(+)} > b_{j(-)}$ or even $b_{j(+)} \gg b_{j(-)}$, whereas the former phenomenon may be captured by adjusting the juxtaposition densities $\rho_{j(+)}$, $\rho_{j(-)}$, and/or the $b_{j(-)}\rho_{j(-)}/b_{j(+)}\rho_{j(+)}$ ratio in the model. The prospect of using this approach for further theoretical progress is promising. Indeed, the fact that $b_{j(\pm)}$ and $\rho_{j(\pm)}$ in our model affect the steady-state average linking number but not its standard deviation fits well conceptually with the experimental deduction that 'topology simplification and chiral sensing employ different mechanism' [19, 61]. However, a detailed exploration of possible models for topoII chiral sensing is beyond the scope of the present work. We focus only on R_{Lk} and do not consider further $b_{j(\pm)}$, $\rho_{j(\pm)}$, or $\langle Lk\rangle_{\rm st}$ below.

3. Results

3.1. Theory rationalizes diminishing R_{Lk} with decreasing DNA circle size

We first consider Lk distribution narrowing by selective strand passage at the specific hooked and half-hooked juxtaposition defined above. The dependence of R_{Lk} on ionic strength and DNA circle size is shown in figure 3. At physiological ionic strength ([NaCl] = 0.154 M), strand passage at the hooked juxtaposition leads to $R_{Lk} \approx 1.7$ for DNA circle size $\gtrsim$4 kb. This level of supercoil relaxation is largely in line with experiment [19, 32] (figure 3(a)). By comparison, the half-hooked juxtaposition attains a lower $R_{Lk} \approx 1.45$ for the same DNA circles. R_{Lk} is reduced by lowering ionic strength. At [NaCl] = 0.01 M, R_{Lk} for the hooked and half-hooked juxtapositions are decreased slightly to $R_{Lk} \approx 1.6$ and 1.35 respectively. It is instructive to recall that the R_{Lk} attained by our lattice model is only 1.28 for the hooked and 1.31 for the twisted-hooked juxtaposition [38]. In light of the present results, these low R_{Lk} values in the lattice model are consistent with our understanding that the behaviour of simple cubic lattice models of DNA is similar to that of more realistic models of DNA at low ionic strengths [52].

Notably, the predicted trend of [NaCl] dependence for R_{Lk} is opposite to that for topoII-mediated unknotting and decatenation. In contrast to a very gradual decrease in R_{Lk} with

decreasing ionic strength (from $R_{Lk} \approx 1.68$ at [NaCl] = 1 M to $R_{Lk} \approx 1.54$ at [NaCl] = 0.01 M; figure 3(*b*)), we found in the same wormlike model that lowering ionic strength causes a dramatic increase in the knot reduction factor R_K and catenane (link) reduction factor R_L for the hooked juxtaposition. A trend in the same direction was observed also for the half-hooked juxtaposition but the increase in simulated R_K and R_L with decreasing [NaCl] is only very gradual for the half-hook [37]. These predictions are in principle testable experimentally, inasmuch as it is possible to restrict the effect of varying ionic strength to the DNA but not the topoII nor the topoII-DNA interaction. In a recent experimental study of topoII supercoil relaxation of 7.9 kb DNA circles, an essentially constant $R_{Lk} = 1.6$ was observed for [KCl] ranging from 0.01 to 0.3 M [24]. These experimental data are not inconsistent with the very gradual decrease of R_{Lk} with decreasing ionic strength that we predicted in figure 3(*b*).

The dependence of R_{Lk} on DNA circle size is also opposite to that of R_K and R_L. The simulated R_{Lk} decreases with decreasing circle size below $\approx$ 3.5 kb (figure 3(*a*)). This predicted behaviour is largely in agreement with experiment [19, 32], though the discrete nature of Lk—which is taken into account here in equations (4) and (5) but not fully in the computation of R_{Lk} from the Gaussian approximation equation (7)—may also affect the experimental R_{Lk} of very small DNA circles [19]. In contrast, using the same wormlike model, we found a dramatic increase in R_K and R_L with decreasing circle size for the hooked juxtaposition. A similar trend was seen for the half-hooked juxtaposition though the corresponding increases in R_K and R_L are much less dramatic [37]. The increasing trend of R_K and R_L with decreasing DNA circle size is consistent with earlier lattice-model results [33, 34] and the original experiment of Rybenkov *et al* [10].

A decreasing R_{Lk} for small DNA circles is a logical consequence of the hooked juxtaposition hypothesis, as has been analyzed in a lattice model [38]. The key insight follows from the basic relation $R_{Lk} \sim \langle Wr \rangle_{00,j}$, where j is the selected juxtaposition (Model and methods). A hooked juxtaposition causes writhe the contributions from different parts of a small circle to cancel largely, netting a small Wr and thus a small R_{Lk} [38]. Hence, the experimental observation of decreasing R_{Lk} for small DNA circles supports the hooked juxtaposition hypothesis. In this respect, further experimental tests of the predicted opposite trends of R_{Lk} versus R_K, R_L in small DNA circles would be extremely instructive.

3.2. Disentangling activity determined by the selected juxtaposition geometry

A broader view of how juxtaposition geometry affects R_{Lk} is provided in figure 4 by varying the geometrical parameters in figure 1. A similar variation of hooked and half-hooked geometries has already been applied to study the knot reduction factor R_K [37]. Figure 4 shows that the hooked geometry—two equal-length segments curving toward each other with the same curvature—is significantly more effective in relaxing supercoils than the half-hooked geometry that contains a straight segment. R_{Lk} is quite insensitive to variation in the segment-segment distance d (figure 4(*a*)). The sensitivity of R_{Lk} on d here is even milder than that of R_K, of which a weak dependence on d was seen within a distance about two times the length l of the DNA segment recognized by topoIIs [37]. This result suggests that the disentangling power of a topoII hinges much more on the curvature of the selected T-segment and/or the crossing angle between the T- and G-segments (see below) rather than the precise distance from the G-segment at which the T-segment is captured by the enzyme.

The trend for the crossing angle θ in figure 4(*b*) indicates that R_{Lk} is enhanced significantly when the T-,G-segment crossing deviates from a right angle. A similar trend of significant increase in R_K with decreasing θ from 90° has already been observed [37]. These results are consistent with our lattice-inspired idea that selective strand passage at twisted-hooked juxtapositions are more disentangling than at hooked juxtapositions, offering a rationalization for the possibility that specific crossing angles between T- and G-segments are recognized by real topoIIs [12, 14]. The symmetry of the '$j(+)$ and $j(-)$' R_{Lk} values here with respect to $\theta = 90°$ is a result of our model assumption that whenever a juxtaposition $j(+)$ with a crossing angle θ is selected for strand passage, the juxtaposition $j(-)$ with the same geometry but has crossing angle $180° - \theta$ is also selected (figure 1(*c*)).

Figure 4(*c*) shows that R_{Lk} is small when l is small but R_{Lk} plateaus out at $l \approx 10$ nm and then declines gradually. R_K also peaks at around the same $l \approx 10$ nm, and decreases more rapidly for larger l [37]. These results suggest that the ~10 nm-length of G-segments found to be interacting with real topoIIs is close to the theoretical optimum.

Supercoil-relaxing power increases with the subtending angle α of the curve segment(s) of the selected juxtaposition (figure 4(*d*)). An even sharper (exponential) increase in R_K with α was observed [37]. Thus disentangling power in general increases with α.

3.3. Scaling of unknotting and decatenating activities with R_{Lk}

The consequences of the above variation in juxtaposition geometry are summarized in figure 5. To broaden our perspective further, we also include in the scatter plots R_{Lk}, R_K, and R_L factors that are smaller than unity because their juxtapositions has $\alpha < 0$. The main correlation relation we obtain by altering d, θ, and varying α over an expanded range (circles in figure 5) is

$$(R_{Lk} - 1) \approx 0.42 \log_{10} R_K \approx 0.68 \log_{10} R_L \qquad (10)$$

as shown in figures 5(*a*) and (*b*), and thus

$$R_K \approx (R_L)^{1.6} \qquad (11)$$

as illustrated in figure 5(*c*). Quite remarkably, this scaling relation[5] is essentially identical to that showcased by the experiment of Rybenkov *et al* [10] (red stars in figure 5).

[5] Most of the simulated R_K and R_L factors in the present analysis were taken from [37]. It should be noted that the relation $R_K \approx (R_L)^{2.0}$ stated in [37] for our wormlike DNA model was based solely on visual inspection. It should be superseded by the present equation (11) from least-squares fitting.

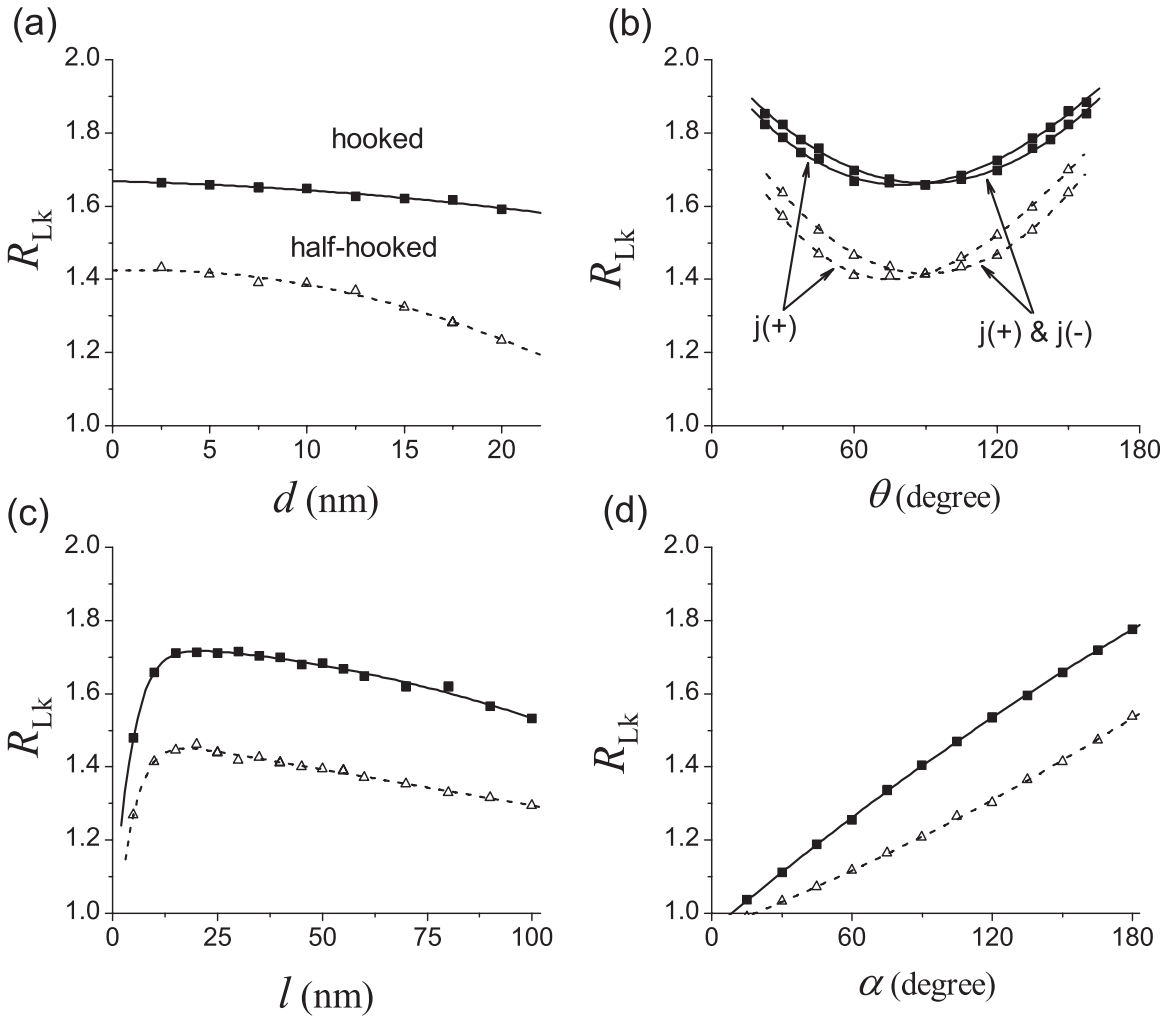

Figure 4. Effects of juxtaposition geometry on the narrowing of Lk distribution by selective strand passage. Simulated R_{Lk} values for 3.5 kb DNA circles and [NaCl] = 0.154 M are shown for variations of the hooked (filled squares) and half-hooked (open triangles) juxtapositions by changing the following parameters one at a time: (*a*) d, (*b*) θ, (*c*) l, and (*d*) α (see figure 1). Except for the parameter being varied in each panel, $d = 5$ nm, $\alpha = 150^\circ$, $\theta = 90^\circ$, and $l = 10$ nm. For all results shown here except the '$j(+)$' data points in (*b*), a selected $j(+)$ with crossing angle θ is paired with a $j(-)$ with crossing angle $180^\circ - \theta$ (Model and methods). For the '$j(+)$' data points in (*b*), which is shown as a control, a selected $j(+)$ with crossing angle θ is paired with a $j(-)$ with crossing angle θ. The minimum R_{Lk} is shifted to $\theta < 90^\circ$ in this prescription, but the general trend of dependence of R_{Lk} on θ is largely unchanged otherwise.

The juxtaposition-centric algorithms we developed [33, 34, 52] have allowed for efficient exploration of a large number of juxtapositions in the wormlike model. There is room for the range of geometries explored to be further extended in future studies. For example, in view of recent experiments showing that G-segment curvature is similar among topoIIs that have significantly different disentangling powers [20, 25], it would be interesting to study a set of juxtapositions that pair a constant-curvature segment with segments of different curvatures. Judging from the trend seen in the exhaustive exploration of juxtaposition geometries in the lattice model [33, 38], however, there is good reason to expect that the additional data points would conform to the scaling seen here.

The outliers in figure 5 that do not fit the scaling relation in equations (10) and (11) also deserve attention. The main outliers in figures 5(*a*) and (*b*) are data points from varying DNA circle size (blue triangles). They are caused by the opposite trend of circle size dependence of R_{Lk} versus R_K and R_L, as noted above. In contrast, the good correlation between $\log R_K$ and $\log R_L$ persists for small circles (given by the high R_K and R_L values in figure 5(*c*)), though the approximate scaling $R_K \approx (R_L)^\nu$ may shift to $\nu > 1.6$ for small circles. Another set of outliers is from varying ionic strength of the solvent (green squares). As also noted above, R_{Lk} decreases gradually with decreasing [NaCl] whereas R_L and R_K exhibit an opposite trend; but this anticorrelation is not as prominent as that caused by varying DNA circle size. Again, as for varying DNA circle size, the good correlation between $\log R_K$ and $\log R_L$ is maintained over the range of [NaCl] values simulated. The third set of outliers arises from varying the segment length l of the juxtaposition (brown diamonds). Interestingly, the good correlation between R_{Lk} and $\log R_K$ is preserved over variations of l, consistent with the similarity between figure 4(*c*) here and figure 3(*c*) of [37]. However, catenane reduction is much less sensitive to variation in l than

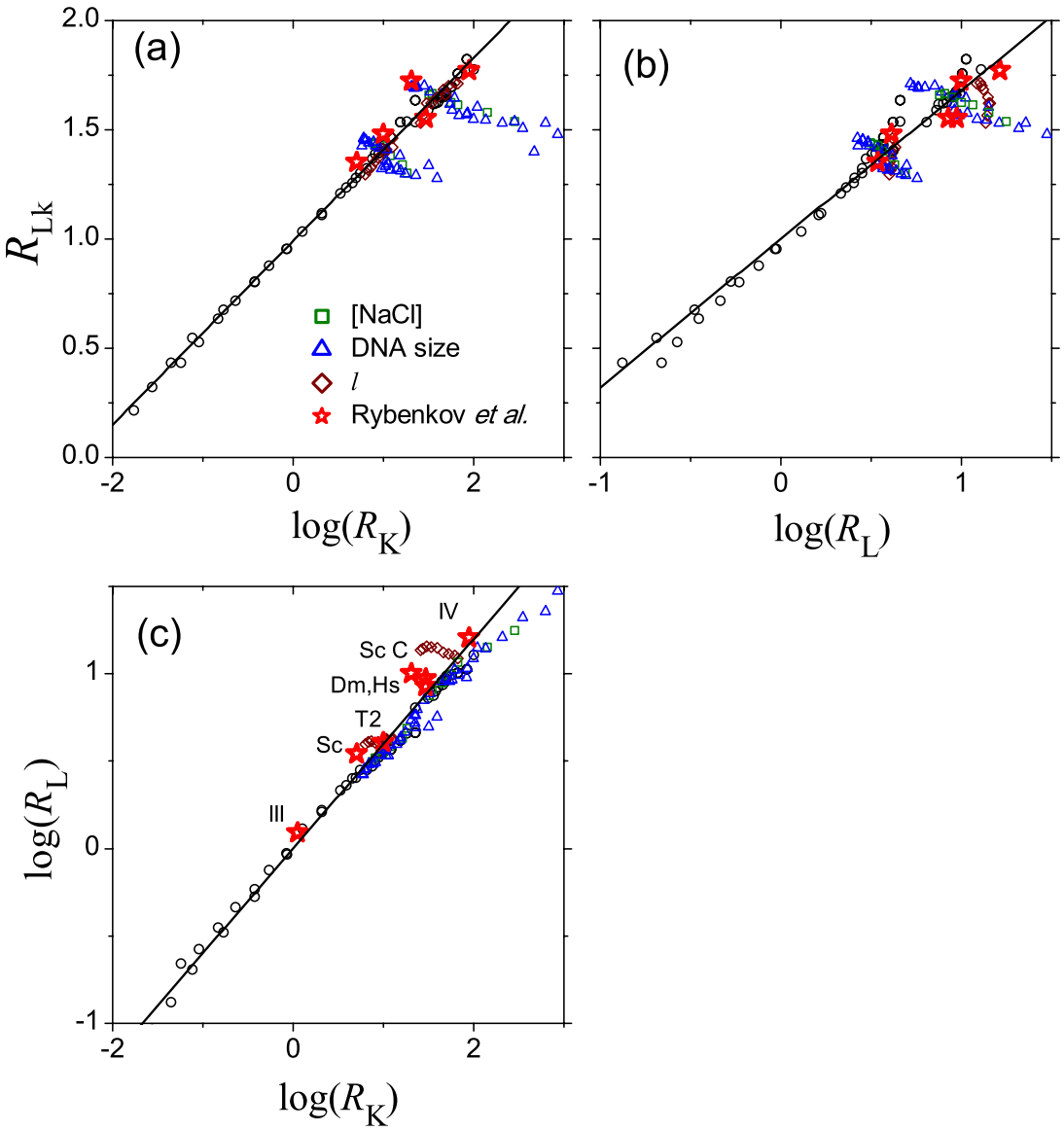

Figure 5. Scaling relation among R_{Lk}, R_K, and R_L. Scatter plots of (a) R_{Lk} versus $\log_{10} R_K$, (b) R_{Lk} versus $\log_{10} R_L$, and (c) $\log_{10} R_L$ versus $\log_{10} R_K$ are shown for R_{Lk}, R_K, and R_L computed from variations of juxtaposition geometry. Circles are data points obtained by varying d, θ, and α while keeping $l = 10$ nm, DNA circle size = 3.5 kb, and [NaCl] = 0.154 M constant. These variations include $\alpha < 0$ cases corresponding to free juxtapositions [37] and 'reverse' half-hooked juxtapositions with a segment curving outward. The least-squares lines fitted to these data points are (x, y denote the horizontal and vertical variables respectively): (a) $y = 0.42x + 0.99$, (b) $y = 0.68x + 1.0$, and (c) $y = 0.61x - 0.02$. Data points obtained by varying ionic strength, DNA size, and segment length l are shown, respectively, by green squares, blue triangles, and brown diamonds. Included for comparison are experimental R_{Lk}, R_{kn} and R_{cat} (red stars) from Rybenkov *et al* for 7 kb DNA circles acted upon by six type-2 topoisomerases (labeled in (c)): topoisomerase IV from *E. coli* (IV), the phage T2 topoisomerase (T2), full-length (Sc) and truncated (Sc C) topoIIs from *Saccharomyces cerevisiae*, topoII from *D. melanogaster* (Dm), and topoII from human cells (Hs); with data for a type-1 topoisomerase III from *E. coli* (III) serving as a control (from figure 3 in [10]). Note that their R_{kn} and R_{cat} are defined very similarly as our R_K and R_L, respectively [34], and that no R_{Lk} was reported for III in [10].

either supercoil relaxation and unknotting, hence the outlying behaviour of the brown data points in figures 5(b) and (c).

4. Discussion and conclusion

4.1. The key insight of the hooked-juxtaposition hypothesis is that selection of curvature is necessary for both the G- and T-segments

The good agreement seen in figure 5 between theoretically predicted and experimentally observed scaling among R_{Lk}, R_K, and R_L is a strong indication that topoIIs perform strand passages at selected DNA juxtapositions. This implication is *more fundamental* than the hooked-juxtaposition hypothesis because the scaling relation applies to a diverse set of juxtapositions, including free juxtapositions that can complicate rather than simplify topology [37]. Within this general framework, the hooked-juxtaposition hypothesis is favoured by experiment because it appears that only juxtapositions with hook-like geometries—rather than half-hooks—can beget disentangling power comparable to that observed in some real topoIIs. For instance, figure 4(b) shows

that with reasonable variations of the crossing angle θ, hooked juxtapositions can reach R_{Lk} values of ≈ 1.8, as observed in experiments [10, 19, 32], whereas half-hooked juxtaposition cannot.

The predicted scaling in figure 5 offers challenges and opportunities to experimentalists. First, it is desirable to obtain more experimental data to evaluate this general prediction. Unknotting and decatenation data are particularly needed. Subsequent to the experiments of Rybenkov *et al* [10], most experimental studies on topoII actions have focused only on supercoil relaxation. Although the unknotting/decatenating activities of topoIIs do correlate well with their supercoil-relaxing acitivities, that is not always the case—especially with regard to small DNA circles (figures 3 and 5). More experiments on unknotting and decatenation will deepen our understanding of the correlation among R_{Lk}, $R_{\rm K}$, $R_{\rm L}$, and lack thereof. Second, the theoretical scaling can also serve to motivate exploration, by protein engineering, of the 'unnatural' regime where R_{Lk}, $R_{\rm K}$, $R_{\rm L} < 1$. Disentangling activity of topoIIs can be reduced experimentally by mutation [17] and by addition of a reagent that interferes with T-segment passage and backtracking [24]. An intriguing recent observation is that the distribution of Lk becomes wider, rather than narrower, when the backtracking process of captured T-segment is blocked [24], thus corresponding possibly to a $R_{Lk} < 1$ situation. It would be an exciting advance in biophysics and biomolecular engineering if by tinkering with the preferred curvature, crossing angle, and other properties of the G- and T-segments selected by topoII mutants, they can be co-opted to complicate rather than simplify DNA topology.

4.2. Topological discrimination by a hooked-juxtaposition mechanism does not require curved G- and T-segments to be recognized simultaneously

It is important to realize that the unknotting and decatenating power in the proposed hooked-juxtaposition mechanism does not require the two segments of the juxtapositions to be recognized simultaneously by topoII. The statistical mechanics of the hooked-juxtaposition hypothesis is agnostic as to whether the two segments are recognized at the same time or not. The hypothesis simply posits—as has been verified computationally—that the occurrence of a juxtaposition at any moment in time, *as long as it is under equilibrium condition*, is sufficient basis for topological discrimination if strand passage is effectuate at that point in time. It does not matter much if the topoII enzyme first recognizes a curved G-segment and then wait for a curved T-segment to drift into position for capture and passage. As we have pointed out briefly before [34], essentially the same mathematical derivation for $R_{\rm K}$ and $R_{\rm L}$ applies to the case in which the entire juxtaposition is recognized simultaneously and the situation that one segment is first recognized and bound by topoII before the other segment is recognized to effectuate the segment passage. For clarity, using notation similar to that in [34], the derivation for $R_{\rm K}$ in the latter situation is provided as follows.

Let $(P_{\rm U})_{\rm eq}$ and $(P_{\rm K})_{\rm eq}$ be the unconstrained equilibrium unknot (U) and knot (K) populations, respectively. Let $(P_{\rm U}^{[j/2]})_{\rm eq}$ and $(P_{\rm K}^{[j/2]})_{\rm eq}$ be the number of appearances of one segment of a specific juxtaposition geometry j (a half-juxtaposition, e.g. when a chain segment is constrained to be a topoII-bound curved G-segment); and $(P_{\rm U}^{(j)})_{\rm eq}$ and $(P_{\rm K}^{(j)})_{\rm eq}$ be the number of instances of the full two-segment juxtaposition j, respectively, in the equilibrium U and K populations.[6] We assume as in [34] that the ratio between the number of instances of half-juxtaposition $[j/2]$ and the number of instances of the full juxtaposition j for unknotted conformations is given by a constant coefficient $c^{(j)}_{{\rm U},[j/2]} \equiv (P_{\rm U}^{(j)})_{\rm eq}/(P_{\rm U}^{[j/2]})_{\rm eq}$. This is the probability of finding a full juxtaposition among the unknotted conformations that already have a half-juxtaposition. A similar coefficient $c^{(j)}_{{\rm K},[j/2]} \equiv (P_{\rm K}^{(j)})_{\rm eq}/(P_{\rm K}^{[j/2]})_{\rm eq}$ is defined for the K population. Thus, the steady-state U and K populations $(P_{\rm U})_{\rm st}$ and $(P_{\rm K})_{\rm st}$ maintained by a two-stage process in which a half-juxtaposition $[j/2]$ is first recognized and bound (fixed) prior to strand passage upon the appearance of the full juxtaposition j at the bound position is then given by the steady-state condition

$$c^{(j)}_{{\rm U},[j/2]}(P_{\rm U})_{\rm st}T^{(j)}_{{\rm U}\to{\rm K}} = c^{(j)}_{{\rm K},[j/2]}(P_{\rm K})_{\rm st}T^{(j)}_{{\rm K}\to{\rm U}}\ , \qquad (12)$$

where $T^{(j)}_{{\rm U}\to{\rm K}}$ and $T^{(j)}_{{\rm K}\to{\rm U}}$ are transition probabilities, respectively, from unknot to knot and from knot to unknot. Therefore, using the relations $\mathcal{J}^{(j)}_{{\rm U}\to{\rm K}} = (P_{\rm U}^{(j)})_{\rm eq}T^{(j)}_{{\rm U}\to{\rm K}}$ and $\mathcal{J}^{(j)}_{{\rm K}\to{\rm U}} = (P_{\rm K}^{(j)})_{\rm eq}T^{(j)}_{{\rm K}\to{\rm U}}$ where $\mathcal{J}^{(j)}_{{\rm U}\to{\rm K}}$ and $\mathcal{J}^{(j)}_{{\rm K}\to{\rm U}}$ are normalized probabilities, respectively, of U→K and K→U segment-passage events [34], the knot reduction factor $R_{\rm K}^{[j/2]}$ in the two-stage process is given by

$$\begin{aligned} R_{\rm K}^{[j/2]} &\equiv \frac{(P_{\rm U})_{\rm st}}{(P_{\rm K})_{\rm st}}\frac{(P_{\rm K})_{\rm eq}}{(P_{\rm U})_{\rm eq}} = \frac{c^{(j)}_{{\rm K},[j/2]}T^{(j)}_{{\rm K}\to{\rm U}}}{c^{(j)}_{{\rm U},[j/2]}T^{(j)}_{{\rm U}\to{\rm K}}}\frac{(P_{\rm K})_{\rm eq}}{(P_{\rm U})_{\rm eq}} \\ &= \frac{\mathcal{J}^{(j)}_{{\rm K}\to{\rm U}}}{\mathcal{J}^{(j)}_{{\rm U}\to{\rm K}}}\frac{(P_{\rm U}^{[j/2]})_{\rm eq}}{(P_{\rm K}^{[j/2]})_{\rm eq}}\frac{(P_{\rm K})_{\rm eq}}{(P_{\rm U})_{\rm eq}}\ . \end{aligned} \qquad (13)$$

Because our original knot reduction factor assuming simultaneous recognition of the entire juxtaposition is given by $R_{\rm K} = \mathcal{J}^{(j)}_{{\rm K}\to{\rm U}}/\mathcal{J}^{(j)}_{{\rm U}\to{\rm K}}$ [34], It follows that

$$R_{\rm K}^{[j/2]} = R_{\rm K}\frac{(P_{\rm U}^{[j/2]})_{\rm eq}}{(P_{\rm K}^{[j/2]})_{\rm eq}}\frac{(P_{\rm K})_{\rm eq}}{(P_{\rm U})_{\rm eq}}\ . \qquad (14)$$

As discussed before [34], since the fractional knot population is small in both the unconstrained ensemble and the ensemble with a half-juxtaposition, and that the fractional knot population is only slightly larger in the latter than in the former, i.e. $(P_{\rm K})_{\rm eq}/(P_{\rm U})_{\rm eq} \lesssim (P_{\rm K}^{[j/2]})_{\rm eq}/(P_{\rm U}^{[j/2]})_{\rm eq} \ll 1$, the approximate equality $R_{\rm K}^{[j/2]} \approx R_{\rm K}$ holds, with $R_{\rm K}^{[j/2]}$ slightly smaller than $R_{\rm K}$. A similar derivation applies to the two-stage catenane reduction factor $R_{\rm L}^{[j/2]}$ and the original $R_{\rm L}$. The implication of a two-stage process on supercoil relaxation is less clear because the derivation of R_{Lk} involves multiple Lk

[6] Although $(P_{\rm U}^{[j/2]})_{\rm eq}$, $(P_{\rm K}^{[j/2]})_{\rm eq}$, $(P_{\rm U}^{(j)})_{\rm eq}$, and $(P_{\rm K}^{(j)})_{\rm eq}$ were referred to as 'conformational populations' in [34], these quantities have always been constructed as counts of the number of half- or full juxtapositions, not the number of conformations per se. In other words, these $P^{[j/2]}$ or $P^{(j)}$ quantities count a half- or full juxtaposition multiple times if it appears multiple times in a single conformation.

states. Nonetheless, in view of the insensitivity of R_{Lk} to d in figure 4(a), it is not unreasonable to expect that a short lag time between the binding of G- and T-segments would not have a serious detrimental effect on supercoil relaxation. But the impact of a long lag time on R_{Lk} is unknown; and this is an important theoretical issue to be resolved.

4.3. Consideration of equilibration kinetics is required to assess proposed mechanisms involving active bending of the G-segment

The above-described two-stage mechanism envisions that the two segments of a selected juxtaposition are recognized separately by the topoII, allowing for a possibly long lag time between binding of the G-segment and capture/passage of the T-segment. Both binding/capturing events are assumed to involve essentially passive recognition of pre-existing DNA conformational geometries by the topoII enzyme, in accordance with the paradigm that a central role in DNA-protein interaction is played by the structures that the DNA adopts by itself [62]. Intuitively, a 'bind, sit and wait' two-stage topoII mechanism may provide kinetic advantage over a mechanism requiring simultaneous recognition of the entire juxtaposition because the occurrence of a full hooked juxtaposition can be rare [36], although the degree of this presumed advantage has yet to be ascertained by simulation of DNA dynamics. As discussed above, the two alternative hooked-juxtaposition mechanisms lead to very similar disentangling outcomes, as least for unknotting and decatenation. Thus, the question as to whether one mechanism is favoured over the other or both mechanisms are operative is best answered by future experiments.

In contrast to passive recognition, the bend-angle model envisions *active bending* of the DNA by the topoII [26, 28, 30, 36]. Recent experiments suggest that topoII may, to a degree, bend/distort the DNA double helix (see, e.g. [21] and references therein). In the biomolecular context, however, the distinction between passive recognition and active bending is not clear cut. Because of thermal fluctuation and structural plasticity, a strictly passive, lock-and-key-like recognition is physically untenable. Indeed, a range of binding mechanisms [63] exists between the idealized 'induced fit' [64] and 'conformational selection' [65] scenarios. Active bending and passive recognition are more akin, respectively, to the induced-fit and conformational-selection scenarios. Nonetheless, despite the possibility of intermediate binding scenarios between these two extremes, there is an obvious physical difference between the proposed active-bending and passive-recognition pictures even if these hypothesized topoII-DNA recognition/binding processes are perceived in broader terms. The proponents of the bend-angle model probably envisioned an even more active role played by the topoII in changing the local DNA conformation than a typical induced-fit situation. In their view, 'simplification of DNA topology would not result if the enzymes bind DNA without distortion' [28]. In essence, the active bending picture posits that a local curvature of the DNA is imposed by the topoII, to the extent that a DNA hairpin can be created from a straight DNA segment. How would this proposed active-bending mechanism affect topological discrimination vis-à-vis the passive-recognition picture that does not ascribe such a task to the topoII?

The proposed active bending perturbs the conformational equilibrium of the DNA. But this equilibrium is the foundation for the topological information embodied in hooked, half-hooked, and for that matter, all juxtapositions. If there is sufficient lag time between active bending of the G-segment and the capture of the T-segment to allow the DNA conformational ensemble to re-equilibrate, the topological discrimination achieved by the subsequent strand passage would be identical to that of the two-stage passive recognition mechanism. This is the basis of our assessment of the effectiveness of the bend-angle model by determining the disentangling power of the half-hooked juxtaposition, which in the absence of T-segment selection appears to be insufficient to match the corresponding experimental values [33, 34, 37, 38] (see also the R_{Lk} results for the half-hook above).

However, if the lag time is insufficient for re-equilibration, there is no guarantee that the strand passage would provide topological discrimination. Imagine a pre-existing juxtaposition with two straight segments. If the hypothetical topoII bends one of the segments into a hairpin and effectuate a strand passage immediately thereafter, the topological discrimination of this process would not be that of a half-hook but rather that of the original pre-existing straight juxtaposition, which provides essentially no topological signal [37, 38]. In view of this consideration, the disentangling power of a two-stage mechanism that involves active bending is expected to be lower than that given by equation (14). In this sense, active bending adds noise to topological discrimination.

Therefore, although active bending can be helpful for the hooked-juxtaposition mechanism by endowing the topoII with the ability to create a curved G-segment or increase the curvature of pre-existing putative G-segment, the presumed kinetic and topological advantage of such a feat [36] has to be balanced against a potential degradation of topological information because of the perturbing effect of active bending on the DNA conformational equilibrium. Enforcing a large change in DNA curvature is energetically costly and will require more lag time for re-equilibration. While the nature of this theoretical tradeoff will have to be assessed by simulation of DNA dynamics, the presumed scarcity of DNA juxtapositions [36] is probably much less of an issue in the cellular context because of supercoiling [55, 56, 58].

4.4. Concluding remarks

To recapitulate, statistical physics and mathematics are essential in deciphering how topoIIs perform their biological functions. In fact, it is not an overstatement that theory has been prophetic in this field. The requirement for topoII to act on a bent DNA segment was put forth by theoreticians advocating either for the bend-angle model [26, 28, 30] or the hooked-juxtaposition hypothesis [31, 33, 34, 54] well before such a bent G-segment was discovered by experimentalists [13]. Here we have presented new computational results in a realistic

DNA chain model. The hypothesis that topoIIs act on hook-like juxtapositions with specific geometries accounts quantitatively for a broad range of experimental data, including a striking scaling relation between the enzymes' unknotting, decatenating and supercoil-relaxing activities. In this light, diversity in disentangling activity among different topoIIs is envisioned to arise from variations in selected T- and G-segment curvature and crossing angle. This prediction is testable by experimental measurements. It is our hope that the quantitative predictions presented would facilitate further theoretical studies as well as spur more experiments and thus contribute to the ultimate solution to the topoII puzzle.

Acknowledgments

This work was supported by the Ministry of Science and Technology of China via grant no. 2015CB910300 to ZL and by the Canadian Institutes of Health Research (CIHR) as well as the Natural Sciences and Engineering Research Council (NSERC) of Canada via CIHR operating grant no. MOP-84281 and NSERC discovery grant no. 216901 to HSC.

References

[1] Delbrück M 1962 *Mathematical Problems in the Biological Sciences* (*Proc. of Symp. in Applied Mathematics* vol 14) (Providence, RI: American Mathematical Society) pp 55–63
[2] Rybenkov V V, Cozzarelli N R and Vologodskii A V 1993 *Proc. Natl Acad. Sci. USA* **90** 5307–11
[3] Podtelezhnikov A A, Cozzarelli N R and Vologodskii A V 1999 *Proc. Natl Acad. Sci. USA* **96** 12974–79
[4] Deibler R W, Rahmati S and Zechiedrich E L 2001 *Genes Dev.* **15** 748–61
[5] Bates A D and Maxwell A 2005 *DNA Topology* (Oxford: Oxford University Press)
[6] Deibler R W, Mann J K, Sumners D W and Zechiedrich L 2007 *BMC Mol. Biol.* **8** 44
[7] Wang J C 1971 *J. Mol. Biol.* **55** 523–33
[8] Wang J C 1996 *Annu. Rev. Biochem.* **65** 635–92
[9] Schoeffler A J and Berger J M 2008 *Q. Rev. Biophys.* **41** 41–101
[10] Rybenkov V V, Ullsperger C, Vologodskii A V and Cozzarelli N R 1997 *Science* **277** 690–3
[11] Hsieh T-J, Farh L, Huang W M and Chan N-L 2004 *J. Biol. Chem.* **279** 55587–93
[12] Corbett K D, Schoeffler A J, Thomsen N D and Berger J M 2005 *J. Mol. Biol.* **351** 545–61
[13] Dong K C and Berger J M 2007 *Nature* **450** 1201–5
[14] Graille M, Cladière L, Durand D, Lecointe F, Gadelle D, Quevillon-Cheruel S, Vachette P, Forterre P and van Tilbeurgh H 2008 *Structure* **16** 360–70
[15] Laponogov I, Sohi M K, Veselkov D A, Pan X-S, Sawhney R, Thompson A W, McAuley K E, Fisher L M and Sanderson M R 2009 *Nat. Struct. Mol. Biol.* **16** 667–9
[16] Laponogov I, Pan X-S, Veselkov D A, McAuley K E, Fisher L M and Sanderson M R 2010 *PLoS One* **5** e11338
[17] Lee I, Dong K C and Berger J M 2013 *Nucl. Acids Res.* **41** 5444–56
[18] Neuman K C, Charvin G, Bensimon D and Croquette V 2009 *Proc. Natl Acad. Sci. USA* **106** 6986–91
[19] Stuchinskaya T, Mitchenall L A, Schoeffler A J, Corbett K D, Berger J M, Bates A D and Maxwell A 2009 *J. Mol. Biol.* **385** 1397–408
[20] Hardin A H, Sarkar S K, Seol Y, Liou G F, Osheroff N and Neuman K C 2011 *Nucl. Acids Res.* **39** 5729–43
[21] Arnoldi E, Pan X-S and Fisher M L 2013 *Nucl. Acids Res.* **41** 9411–23
[22] Seol Y, Hardin A H, Strub M-P, Charvin G and Neuman K C 2013 *Nucl. Acids Res.* **41** 4640–9
[23] Seol Y, Gentry A C, Osheroff N and Neuman K C 2013 *J. Biol. Chem.* **288** 13695–703
[24] Martínez-García B, Fernández X, Díaz-Ingelmo, Rodríguez-Campos, Manichanh C and Roca J 2014 *Nucl. Acids Res.* **42** 1821–30
[25] Thomson N H, Santos S, Mitchenall L A, Stuchinskaya T, Taylor J A and Maxwell A 2014 *Sci. Rep.* **4** 6158
[26] Vologodskii A 1998 *Proc. of the Second Annual Int. Conf. on Computational Molecular Biology* (New York: Association for Computing Machinery) pp 266–9
[27] Yan J, Magnasco M O and Marko J F 1999 *Nature* **401** 932–5
[28] Vologodskii A V, Zhang W, Rybenkov V V, Podtelezhnikov A A, Subramanian D, Griffith J D and Cozzarelli N R 2001 *Proc. Natl Acad. Sci. USA* **98** 3045–9
[29] Yan J, Magnasco M O and Marko J F 2001 *Phys. Rev.* E **63** 031909
[30] Klenin K, Langowski J and Vologodskii A 2002 *J. Mol. Biol.* **320** 359–67
[31] Buck G R and Zechiedrich E L 2004 *J. Mol. Biol.* **340** 933–9
[32] Trigueros S, Salceda J, Bermúdez I, Fernández X and Roca J 2004 *J. Mol. Biol.* **335** 723–31
[33] Liu Z, Zechiedrich E L and Chan H S 2006 *Biophys. J.* **90** 2344–55
[34] Liu Z, Mann J K, Zechiedrich E L and Chan H S 2006 *J. Mol. Biol.* **361** 268–85
[35] Liu Z, Deibler R W, Chan H S and Zechiedrich L 2009 *Nucl. Acids Res.* **37** 661–71
[36] Vologodskii A 2009 *Nucl. Acids Res.* **37** 3125–33
[37] Liu Z, Zechiedrich L and Chan H S 2010 *Phys. Rev.* E **81** 031902
[38] Liu Z, Zechiedrich L and Chan H S 2010 *J. Mol. Biol.* **400** 963–82
[39] Micheletti C, Marenduzzo D and Orlandini S 2011 *Phys. Rep.* **504** 1–73
[40] Sumners D W and Whittington S G 1988 *J. Phys. A: Math. Gen.* **21** 1689–94
[41] Hua X, Nguyen D, Raghavan B, Arsuaga J and Vazquez M 2007 *Topol. Appl.* **154** 1381–97
[42] Szafron M L and Soteros C E 2011 *J. Phys. A: Math. Theor.* **44** 245003
[43] Portillo J, Diao Y, Scharein R, Arsuaga J and Vazquez M 2011 *J. Phys. A: Math. Theor.* **44** 275004
[44] Hong K, No S and Oh S 2013 *J. Phys. A: Math. Theor.* **46** 125001
[45] Cheston M A, McGregor K, Soteros C E and Szafron M L 2014 *J. Stat. Mech.* P02014
[46] Flammini A, Maritan A and Stasiak A 2004 *Biophys. J.* **87** 2968–75
[47] Marenduzzo D, Orlandini E, Stasiak A, Sumners D W, Tubiana L and Micheletti C 2009 *Proc. Natl Acad. Sci. USA* **106** 22269–74
[48] Dorier J and Stasiak A 2013 *Nucl. Acids Res.* **41** 6808–15
[49] Chan H S, Shimizu S and Kaya H 2004 *Methods Enzymol.* **380** 350–79
[50] Chan H S, Zhang Z, Wallin S and Liu Z 2011 *Annu. Rev. Phys. Chem.* **62** 301–26
[51] Sikosek T and Chan H S 2014 *J. R. Soc. Interface* **11** 20140419
[52] Liu Z and Chan H S 2008 *J. Chem. Phys.* **128** 145104
[53] Liu Z and Chan H S 2009 *J. Chem. Phys.* **131** 049902
[54] Burnier Y, Weber C, Flammini A and Stasiak A 2007 *Nucl. Acids Res.* **35** 5223–31
[55] Witz G and Stasiak A 2010 *Nucl. Acids Res.* **38** 2119–33
[56] Witz G, Dietler G and Stasiak A 2011 *Proc. Natl Acad. Sci. USA* **108** 3608–11

[57] Katritch V, Bednar J, Michoud D, Scharein R G, Dubochet J and Stasiak A 1996 *Nature* **384** 142–5
[58] Witz G, Dietler G and Stasiak A 2011 *Cell Cycle* **10** 1339–40
[59] Stone M D, Bryant Z, Crisona N J, Smith S B, Vologodskii A, Bustamante C and Cozzarelli N R 2003 *Proc. Natl Acad. Sci. USA* **100** 8654–9
[60] Fogg J M, Catanese D J, Randall G L, Swick M C and Zechiedrich L 2009 *Mathematics of DNA Structure, Function and Interactions* (*The IMA Volumes in Mathematics and Its Applications* vol 150) ed C J Benham *et al* (Berlin: Springer) pp 73–121
[61] Timsit Y 2011 *Nucl. Acids Res.* **39** 8665–76
[62] Fogg J M, Randall G L, Pettitt B M, Sumners D L, Harris S A and Zechiedrich L 2012 *Q. Rev. Biophys.* **45** 257–99
[63] Csermely P, Palotai R, Nussinov R 2010 *Trends Biochem. Sci.* **35** 539–46
[64] Koshland D E 1958 *Proc. Natl Acad. Sci. USA* **44** 98–104
[65] Závodszky P, Abaturov L V and Varshavsky Y M 1966 *Acta Biochim. Biophys. Acad. Sci. Hung.* **1** 389–402